THE JOURNAL OF BIOLOGICAL CHEMISTRY VOL. 291, NO. 46, pp. 24188–24199, November 11, 2016

Identification of Small Molecule Inhibitors of Human Cytochrome *c* Oxidase That Target Chemoresistant Glioma Cells*[S]

Received for publication, July 22, 2016, and in revised form, September 25, 2016 Published, JBC Papers in Press, September 27, 2016, DOI 10.1074/jbc.M116.749978

Claudia R. Oliva[‡], Tahireh Markert[‡], Larry J. Ross[§], E. Lucile White[§], Lynn Rasmussen[§], Wei Zhang[§], Maaike Everts[¶], Douglas R. Moellering[‖], Shannon M. Bailey[**], Mark J. Suto[§], and Corinne E. Griguer[‡ ‡‡1]

From the [‡]Department of Neurosurgery, [‡‡]Center for Free Radical Biology, and [¶]Department of Pediatrics, Division of Infectious Diseases, University of Alabama at Birmingham, Birmingham, Alabama 35294, [§]Drug Discovery Division, Southern Research, Birmingham, Alabama 35205, [**]Department of Pathology, Division of Molecular and Cellular Pathology, University of Alabama at Birmingham, Birmingham, Alabama 35294, and [‖]UAB Nutrition Sciences Department, Diabetes Research Center BARB Core, University of Alabama at Birmingham, Birmingham, Alabama 35294

Edited by Ruma Banerjee

The enzyme cytochrome *c* oxidase (CcO) or complex IV (EC 1.9.3.1) is a large transmembrane protein complex that serves as the last enzyme in the respiratory electron transport chain of eukaryotic mitochondria. CcO promotes the switch from glycolytic to oxidative phosphorylation (OXPHOS) metabolism and has been associated with increased self-renewal characteristics in gliomas. Increased CcO activity in tumors has been associated with tumor progression after chemotherapy failure, and patients with primary glioblastoma multiforme and high tumor CcO activity have worse clinical outcomes than those with low tumor CcO activity. Therefore, CcO is an attractive target for cancer therapy. We report here the characterization of a CcO inhibitor (ADDA 5) that was identified using a high throughput screening paradigm. ADDA 5 demonstrated specificity for CcO, with no inhibition of other mitochondrial complexes or other relevant enzymes, and biochemical characterization showed that this compound is a noncompetitive inhibitor of cytochrome *c*. When tested in cellular assays, ADDA 5 dose-dependently inhibited the proliferation of chemosensitive and chemoresistant glioma cells but did not display toxicity against non-cancer cells. Furthermore, treatment with ADDA 5 led to significant inhibition of tumor growth in flank xenograft mouse models. Importantly, ADDA 5 inhibited CcO activity and blocked cell proliferation and neurosphere formation in cultures of glioma stem cells, the cells implicated in tumor recurrence and resistance to therapy in patients with glioblastoma. In summary, we have identified ADDA 5 as a lead CcO inhibitor for further optimization as a novel approach for the treatment of glioblastoma and related cancers.

Cytochrome *c* oxidase (CcO,[2] complex IV; EC 1.9.3.1) is the terminal enzyme of the mitochondrial respiratory chain (electron transport chain (ETC)). CcO is a complex enzyme consisting of 13 subunits, 3 of which are encoded by the mitochondrial DNA and perform the catalytic function and 10 of which are nuclear-encoded and provide the regulatory function (1, 2). Through the transfer of electrons from cytochrome *c* (cyt *c*) to oxygen, CcO catalyzes the reduction of molecular oxygen to water and couples the free energy of the reaction to proton pumping across the membrane (3–5). The concurrent translocation of protons further contributes to the established proton electrochemical gradient that is then utilized by ATP synthase to generate ATP from ADP and P_i (4, 5).

Glioblastoma multiforme (GBM) is the most frequent form of high grade malignant brain tumor. Since the study by Stupp *et al.* in 2005 (6 and 7), the standard of care treatment for patients with primary GBM has included a regimen of concomitant and adjuvant chemotherapy with temozolomide (TMZ) (8). Although the chemotherapeutic regimen is commonly used as part of the treatment against GBM and can be advantageous for short periods of time, chemotherapy is eventually impaired by the development of chemoresistance. This phenomenon represents the most challenging problem in the successful treatment of cancer and is the main reason for chemotherapy failure.

Increased levels of CcO activity have been associated with the acquisition of chemoresistance to TMZ in malignant gliomas (9–11). Increased CcO activity augments the electron flux capacity of the ETC, leading to more efficient mitochondrial coupling and reduced production of reactive oxygen species (10–13). These alterations are likely to facilitate adaptive chemoresistance through the suppression of apoptotic signaling (11). We recently demonstrated that high CcO activity

* This work was supported in part by National Institutes of Health Grants R01CA160821 and P30 DK079626. Work reported in this publication was supported by the Alabama Drug Discovery Alliance (ADDA) and collaboration between the University of Alabama at Birmingham and Southern Research Institute as well as the National Center for Advancing Translational Sciences of the National Institutes of Health (National Institutes of Health) under award UL1TR00165. The authors declare that they have no conflicts of interest with the contents of this article. The content is solely the responsibility of the authors and does not necessarily represent the official views of the National Institutes of Health.

[S] This article contains supplemental Table S1 and Fig. S1.

[1] To whom correspondence should be addressed. E-mail: cegriguer@uabmc.edu.

[2] The abbreviations used are: CcO, cytochrome *c* oxidase; ETC, electron transport chain; cyt *c*, cytochrome *c*; GBM, glioblastoma multiforme; TMZ, temozolomide; HTS, high throughput screen; ROC, receiver operating characteristic; XO, xanthine oxidase; LDH, lactate dehydrogenase; SOD, superoxide dismutase; GPx, glutathione peroxidase; GR, glutathione reductase; FCCP, carbonyl cyanide *p*-trifluoromethoxyphenylhydrazone; GSC, glioma stem cell; LM, *n*-dodecyl β-D-maltoside.

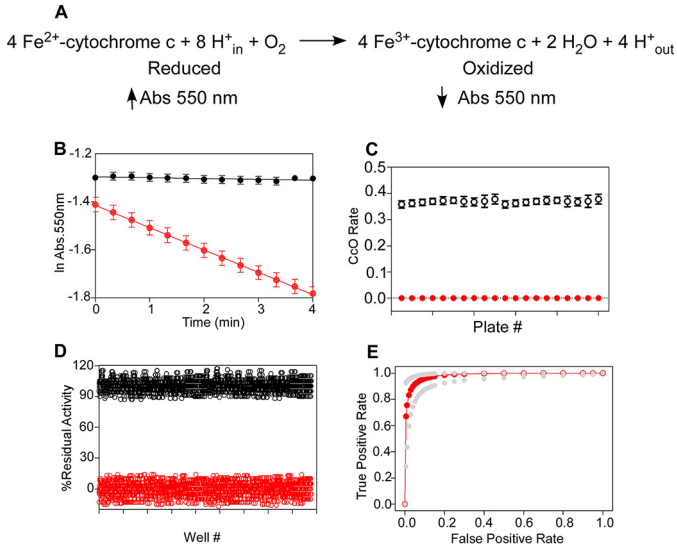

FIGURE 1. **CcO activity assay.** *A*, the reaction scheme depicts the previously published assay (9–11) that was the basis for the HTS. *B*, graph depicting the time course for the optimized assay. *Black circles* represent data from assays performed in the absence of mitochondrial extracts; *red circles* represent data from assays performed with CcO. *C* and *D*, power of HTS assay. The positive controls (*open circles*) and the negative controls (*red circles*) are plotted. The assay shows non-significant batch-to-batch variability (*C*) and a large hit window between high and low controls, with a calculated Z′ factor >0.62 (*D*). *E*, ROC curve for the CcO assay. ROC area under the curve, 0.984. Bootstrap simulation curves are in *light gray*.

within the tumor occurs in a significant subset of patients with high grade gliomas and is an independent predictor of poor outcome (14). We have also demonstrated that inhibition of CcO activity reverses chemoresistance to TMZ *in vitro* (10, 11), supporting a close correlation between acquired chemoresistance and changes in cellular metabolic machinery at the level of the mitochondrion.

Herein, we describe a biochemical absorbance-based high throughput screen (HTS) to identify small molecule inhibitors of CcO. These compounds could serve as tools to investigate the role of CcO in cancer cells and may have direct therapeutic application for treatment of glioblastomas.

Results

Assay Validation and Optimization—A biochemical absorbance-based HTS was developed to identify small molecule inhibitors of CcO in mitochondrial extracts. The CcO assay is a modification of a procedure previously reported (10, 11, 15, 16) and spectrophotometrically monitors the oxidation of cyt *c* by CcO at 550 nm. A schematic outlining the reaction is displayed in Fig. 1*A*. The measured signal is proportional to the amount of cyt *c* remaining after the CcO reaction, so compared with the DMSO control CcO inhibitors produce high signals. CcO activity in mitochondrial extracts was stable at room temperature for 4 h. The optimal mitochondrial extract concentration and the optimal reaction rate were determined in 5-μl reaction volumes in 1536-well plates, with the mitochondrial extract concentration adjusted to provide a linear reaction rate at 550 nm for 4 min. Reproducibility of the full reaction rate for CcO was evaluated by assaying several full 1536-well plates spread out over 4 h. At the optimal mitochondrial extract concentration, reaction rates with R^2 values of 0.998 indicated good linearity during the defined assay time (Fig. 1*B*). The developed assay was found to be linear with respect to both time and the concentration of mitochondrial extracts. Analysis by absorbance also confirmed the batch-to-batch variability was non-significant (Fig. 1*C*). Analysis of the statistical parameter Z′, which defines a measure of the quality of the HTS (17), produced a value of 0.62 (Fig. 1*D*). Specifically, Z′ describes the window between high and low controls by which we can determine our lead "hits"; a well defined hit window is indicated by a value of >0.5 (17). Furthermore, the average activities of each well in all plates screened did not indicate plate well positional trends.

Results of the HTS—In all, 134,855 compounds were initially screened at 10 μg/ml or 30 μM using mitochondrial extracts from TMZ-resistant U251 glioma cells (UTMZ cells). Those compounds that had a cutoff value of >21% inhibition of CcO (1059 compounds) were selected for a 10-point concentration response analysis and a cytotoxicity determination. The discriminatory power of the primary screen was assessed using receiver operating characteristic (ROC) analysis with representative compounds (Fig. 1*E*) (18). True positives were defined as any compound yielding a well behaved, saturating sigmoidal curve in the dose-response assay. ROC analyses indicated excellent discriminatory power with a fitted ROC area under the curve of 0.984 and an empiric ROC area under the curve of 0.978. The accuracy, sensitivity, and specificity of the screen were 93.2%, 90.7%, and 96.5%, respectively. The most promising 163 inhibitors were selected for further analysis on the basis of potency, curve filter, and Hill number.

Synthetic Lethality Screen in Chemoresistant Human Glioma Cells—To identify CcO inhibitors selectively toxic to glioma cells, we performed a secondary screen in a cellular environment using a three cell line-based series of assays. The assay has been automated and validated for HTS, and hits from the primary screen were screened to assess reliability and reproducibility of this assay. To assess selectivity of the identified primary hit compounds, a dose-response study with TMZ-resistant UTMZ glioma cells (10, 11) and the LL-47 fibroblast cell line was conducted, and EC_{50} values for inhibition of proliferation were determined based on the dose-response curve of 0.039 to 20 μg/ml concentrations of each hit compound. In addition to these two assays, compounds were evaluated in U251 glioma cells to identify compounds effective against the parental, drug-sensitive glioma line, and compounds were evaluated in UTMZ cells in the presence of a sub-lethal dose of TMZ to identify compounds that may work synergistically with TMZ in resistant cells. For all assays, cells were incubated with individual compounds at 37 °C for 72 h, and we determined the number of viable cells in culture using the CellTiter-Glo® Luminescent Cell Viability Assay. We calculated the EC_{50} value (concentration required to inhibit 50% of the CellTiter-Glo signal) for each compound in each cell line and thereby identified 20 compounds that were toxic to glioma cells but non-toxic for human fibroblasts (supplemental Table S1).

Hit Confirmation—Because the spectrophotometric assay of CcO activity measures the accumulation of oxidized cyt *c* at 550 nm, cyt *c* reducing agents will give the same results as CcO inhibitors and can thus produce false positive hits. Therefore, we developed and implemented a follow-up assay in which cyt *c*

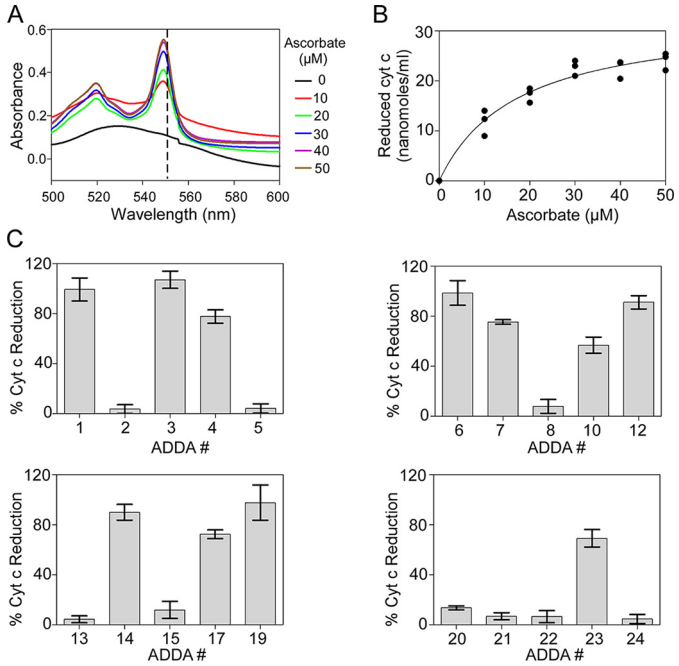

FIGURE 2. **Counter screen for hits confirmation.** *A*, representative visible absorption spectra of oxidized cyt *c* (0 μM ascorbate) and reduced cyt *c* after the addition of the indicated ascorbate concentrations. *B*, dose-response effect of ascorbate on cyt *c* reduction. Reduced cyt *c* concentration (μM) was calculated using absorbance values at 550 nm from the absorption spectra shown in *A* and the cyt *c* molar extinction coefficient of 1.92. Complete cyt *c* reduction was achieved by 40–50 μM ascorbate. *C*, the 20 ADDA compounds toxic to glioma cells (supplemental Table S1) were individually assayed to distinguish cyt *c* reducing compounds from true CcO inhibitors. The visible absorption spectra of cyt *c* after the addition of 50 μM concentrations of each compound was used to determine the percentage of cyt *c* reduction relative to cyt *c* reduction by 50 μM ascorbate (100%). Nine compounds (ADDA 2, 5, 8, 13, 15, 20, 21, 22, and 24) did not reduce cyt *c* and were, thus, selected for further analysis as true CcO inhibitors. Eleven compounds (ADDA 1, 3, 4, 6, 7, 10, 12, 14, 17, 19, and 23) did reduce cyt *c* and were identified as cyt *c* reductants and, therefore, not further investigated as CcO inhibitors.

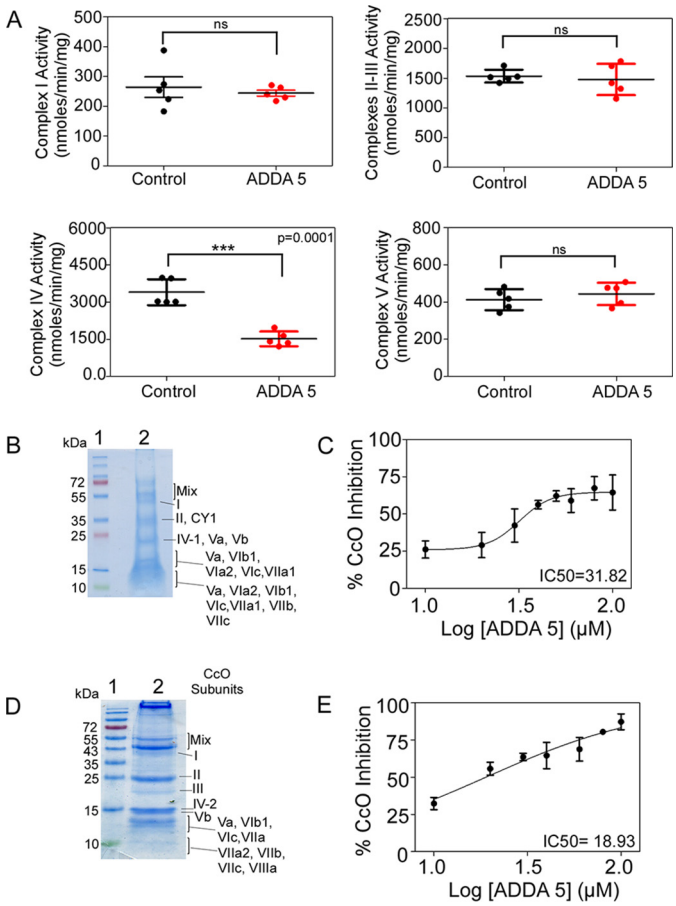

FIGURE 3. **Effects of ADDA 5 on mitochondrial complexes.** *A*, ADDA 5 was tested on mitochondrial extracts from TMZ-resistant glioma cells for effects on the activity of complexes I-III, CcO (complex IV), and complex V of the mitochondrial transport chain. *Scatter graphs* represent the activity level of each complex in the presence of DMSO (*Control*) and ADDA 5 (25 μM). The results are averages from triplicate determinations from two independent experiments. *ns*, not significant; ***, $p < 0.0002$. *B*, representative SDS-PAGE stained with Coomassie Blue. *Lane 1*, protein ladder. *Lane 2*, purified CcO from bovine heart. Band identities were determined by MS. A band label of *Mix* indicates the presence of multiple CcO subunits due to incomplete denaturation of CcO. *C*, effect of ADDA 5 on the activity of purified CcO from bovine heart. ADDA 5 inhibited CcO with an IC_{50} of 31.82 $\pm$ 2.89 μM. *D*, representative SDS-PAGE stained with Coomassie Blue. *Lane 1*, protein ladder. *Lane 2*, purified CcO from human glioma cells. Band identities were determined by MS. A band label of *Mix* indicates the presence of multiple CcO subunits due to incomplete denaturation of CcO. *E*, effect of ADDA 5 on the activity of purified CcO from human glioma cells. ADDA 5 inhibited CcO with an IC_{50} of 18.93 $\pm$ 0.04 μM.

was incubated with the candidate CcO-inhibiting compounds in the absence of purified CcO or mitochondrial extracts to distinguish compounds that directly reduce cyt *c* from those that are likely to be true CcO inhibitors. The visible absorption spectra of cyt *c* was measured with or without the individual addition of the 20 compounds identified by the primary and secondary HTS screenings. Whereas oxidized cyt *c* produces only one peak at 530 nm, a new band at 550 nm indicating reduced cyt *c* was observed upon sodium ascorbate treatment (Fig. 2*A*, positive control). The intensity of the response was dose-dependent, with saturation at 40 μM ascorbate (Fig. 2*B*). Subsequent validation experiments using the same experimental procedure used for ascorbate suggested that 9 of the 20 drugs identified in the initial screening did not reduce cyt *c* in the absence of CcO and are thus likely to be true CcO inhibitors (Fig. 2*C*). We finally prioritized the compounds for further studies by filtering out compounds with an IC_{50} for CcO inhibition >40 μg/ml.

To address the specificity of the remaining hit molecules, we tested the compounds for inhibitory activity against all mitochondrial complex activities. Each of the molecules was tested for the effects on complexes I, II-III, CcO, and complex V of the ETC at the IC_{50} value established by the primary HTS. One compound was identified as an specific inhibitor of CcO and selected for further analysis: ADDA 5, 1-[2-(1-adamantyl)-ethoxy]-3-(3,4-dihydro-2(1H)-isoquinolinyl)-2-propanol hydrochloride] (Fig. 3*A*).

Because ADDA 5 was identified using mitochondrial extracts, we assessed the possibility that the resulting CcO inhibition was a consequence of an indirect effect due to binding to other mitochondrial component(s) by evaluating the effect of ADDA 5 on purified CcO. ADDA 5 was tested against CcO purified from bovine heart (Fig. 3, *B* and *C*) and CcO purified from human glioma cells (Fig. 3, *D* and *E*). By SDS-PAGE, the purified enzymes gave multiple bands of apparent molecular mass ranging from 12 to 55 kDa.

MS-based analysis of each band confirmed the identity of each CcO subunit (Fig. 3, *B* and *D*). ADDA 5 inhibited purified CcO from both species, but CcO from human glioma was the

most sensitive, with an IC_{50} of 18.93 ± 0.04 μM, whereas CcO from bovine heart was inhibited with an IC_{50} of 31.82 ± 2.89 μM.

To further define the specificity of ADDA 5, we next determined whether this compound also inhibits xanthine oxidase (XO), catalase, lactate dehydrogenase (LDH), superoxide dismutase (SOD), glutathione peroxidase (GPx), or glutathione reductase (GR). All these enzymes were suitable controls because they are involved in metabolism and protection against oxidative stress, are found in nearly all mammalian tissues, and are commonly up-regulated in cancer cells. These enzymes were insensitive to ADDA 5 (Fig. 4, *A–F*), suggesting that ADDA 5 selectively inhibits CcO.

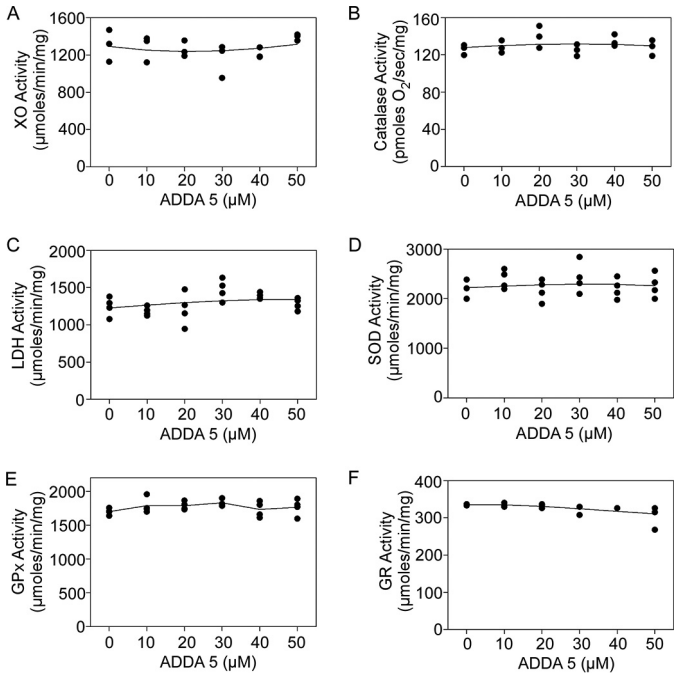

FIGURE 4. **Inhibitory specificity of ADDA 5.** The specificity of ADDA 5 was investigated by testing for inhibition of other enzymes, including XO (*A*), catalase (*B*), LDH (*C*), SOD (*D*), GPx (*E*), and GR (*F*). Activity assays were performed as described under "Experimental Procedures. No inhibition was observed at any tested concentration, suggesting that ADDA 5 is selective for CcO. Scatter plots are the results from duplicate determinations from two independent experiments.

Characterization of CcO Inhibition by ADDA 5—We next investigated the kinetic mechanism of ADDA 5 inhibition of CcO. ADDA 5 lowered the V_{max} but not the K_m for cyt *c*. Fig. 5*A* shows the representative Michaelis-Menten graph, and Fig. 5*B* shows representative Lineweaver-Burk double-reciprocal plots indicating a non-competitive inhibition of cyt *c*, with a 50% decrease in V_{max} at 14 μM ADDA 5. According to the Dixon graphical method, the dissociation constant (K_i) for a CcO-ADDA 5 complex is 16.73 ± 0.20 μM (Fig. 5*C*). Because the maximal CcO inhibition reached a plateau at 60% of the V_{max}, we evaluated whether ADDA 5 is a complete or partial CcO inhibitor. Plotting experimental data as $v/(v_0 - v)$ *versus* the reciprocal of the inhibitor concentration at different substrate concentrations, where v and v_0 represent the velocity in the presence and absence of the inhibitor, respectively, with a given concentration of the substrate, partial inhibition results in straight lines that converge on the abscissa at a point away from the origin, whereas complete inhibition results in lines that go through the origin (19, 20). As shown in Fig. 5*D*, ADDA 5 is a partial non-competitive CcO inhibitor, indicating that binding of ADDA 5 to CcO slows but does not completely prevent catalysis.

Effects of ADDA 5 on Cellular Bioenergetics and Proliferation—Here, we investigated the cellular bioenergetic response to ADDA 5, specifically the oxygen consumption rates of the chemoresistant UTMZ glioma cells by high resolution respirometry. Cells were allowed to establish a stable baseline, and then CcO inhibitors were injected into the sample chamber. Injection of the ATP synthase inhibitor oligomycin caused

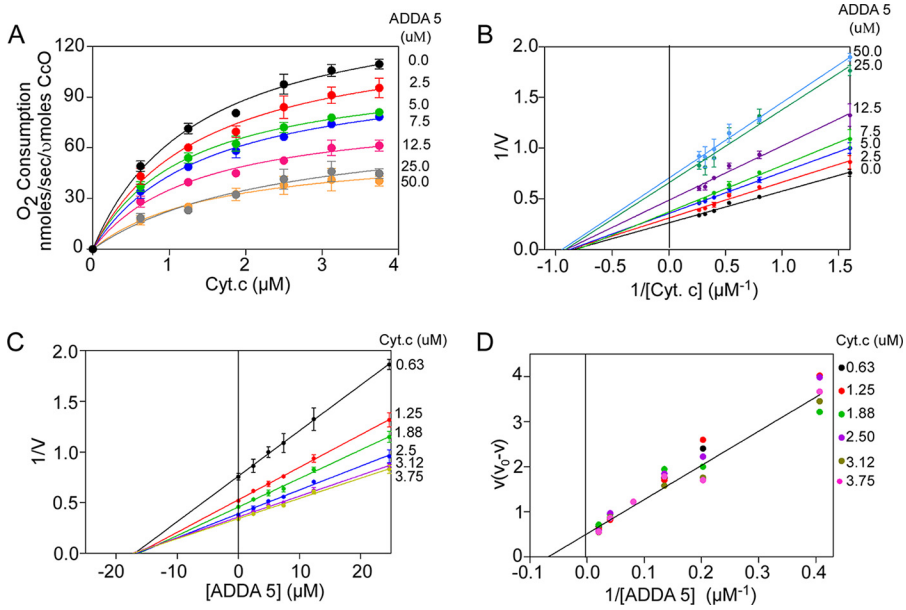

FIGURE 5. **Kinetic mechanism for CcO inhibition by ADDA 5.** *A*, initial rate data for different concentrations of ADDA 5 and cyt *c*. *B*, Lineweaver-Burk double-reciprocal plot. The inhibitor is non-competitive with regard to cyt *c*. *C*, Dixon plot. The K_i for a CcO-ADDA 5 complex is 16.73 ± 0.20 μM. *D*, fractional velocity plots indicate that ADDA 5 is a partial non-competitive inhibitor.

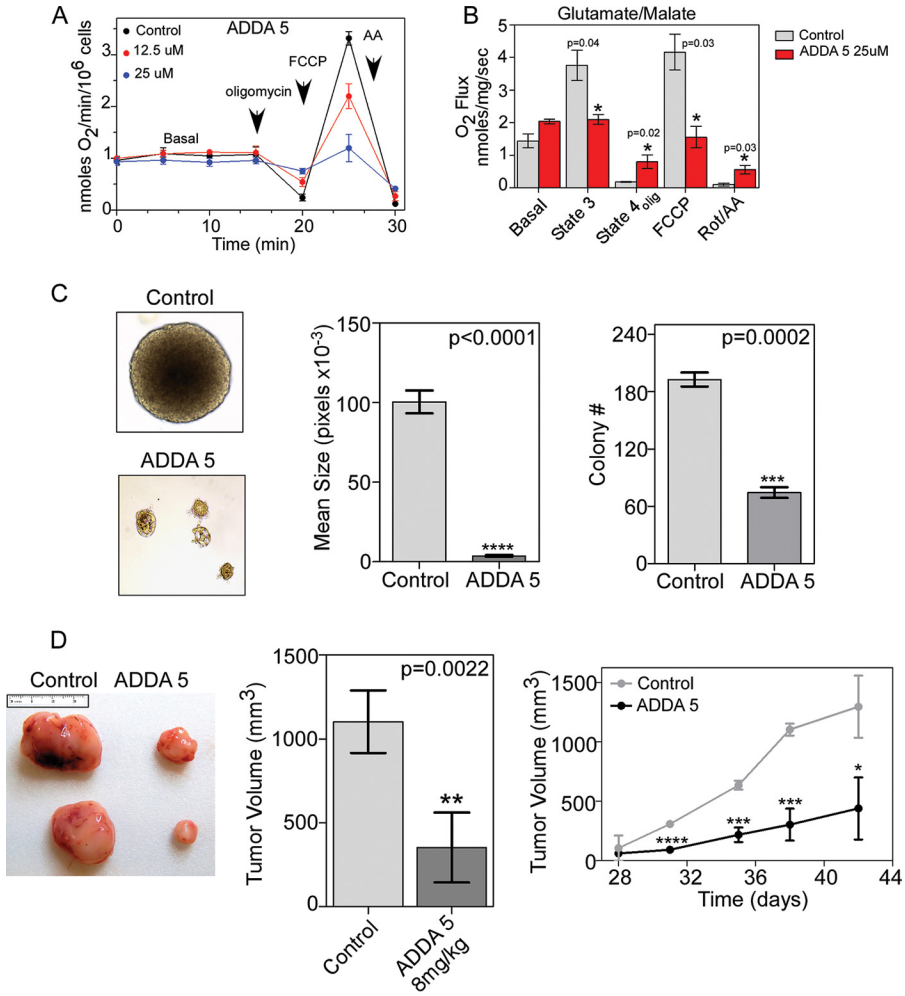

FIGURE 6. **Effect of ADDA 5 on TMZ-resistant cells.** *A*, oxygen consumption in the presence of ADDA 5. The use of specific inhibitors to determine the sites of cellular oxygen consumption is shown. Oligomycin (2 μg/ml), FCCP (1 μM), and antimycin A (*AA*, 10 μM) were injected sequentially, with oxygen consumption measurements recorded after each injection. The reserve respiratory capacity is calculated by subtracting the basal from the maximal rate of oxygen consumption. *B*, kinetic characterization of glutamate/malate-dependent respiration of isolated mitochondria from UTMZ cells in the absence and presence of ADDA 5. Respiration was measured after the addition of 10 mM glutamate and 5 mM malate and DMSO (control) or ADDA 5. Data are expressed as the mean ± S.D. of three independent experiments. *C*, representative pictures of clonogenic assays showing anchorage-independent cell growth of ADDA 5- or vehicle-treated UTMZ cells (*left panel*). Shown is a comparison of colony size (*middle panel*) and colony number (*right panel*) of ADDA 5- or vehicle-treated UTMZ cells. Graphs represent the average from triplicate determinations from two independent experiments. *D*, representative images of tumors from athymic nude mice inoculated with UTMZ cells and treated with ADDA 5 (8 mg/kg) or vehicle, excised 43 days after inoculation (*left panel*). Comparison of tumor weights upon excision (*middle panel*). Analysis of tumor volumes in mice over the course of the experiment (*right panel*) is shown. Graphs represent the average tumor volume from a single study with five mice. $p < 0.05$ (*), $p < 0.01$ (**), $p < 0.001$ (***), and $p < 0.0001$ (****).

a substantial decrease in oxygen flux (rate of respiration) in control cells that was significantly suppressed by ADDA 5 in a dose-dependent manner (Fig. 6*A*). To determine the maximal respiratory capacity, the mitochondrial uncoupler FCCP was injected into the sample chamber, causing an increase in oxygen flux relative to baseline. However, the maximal oxygen consumption after FCCP injection was significantly decreased in the presence of ADDA 5, indicating a loss of reserve capacity. Finally, injection of antimycin A/rotenone significantly inhibited respiration in all groups, with a greater effect on the control DMSO-treated cells.

Fig. 6*B* shows representative values of mitochondrial oxygen consumption, with glutamate and malate as substrates, obtained for respiration states 3 and 4 and for uncoupled respiration in the presence of FCCP. ADDA 5-treated cells had significantly lower state 3 and higher state 4 oxygen consumption rates (2.10 ± 0.11 and 0.80 ± 0.15 nmol O_2/s/mg of protein, respectively) than control-treated cells (3.77 ± 0.33 and 0.18 ± 0.01 nmol O_2/s/mg protein, respectively; $p \leq 0.05$) (Fig. 6*B*). Furthermore, colony-forming assays in UTMZ cells (9–11) confirmed a growth inhibitory effect of ADDA 5. In contrast, DMSO-treated UTMZ cells efficiently formed colonies, reflecting their transformed phenotype (Fig. 6*C*).

Effects of ADDA 5 on Tumor Cells in Vivo—Having established that CcO inhibition has an effect on glioma cell proliferation, we evaluated the ability of ADDA 5 to inhibit the growth of UTMZ cells in the flanks of nude mice. Before conducting these efficacy studies, we established an acute toxicity profile, administering ADDA 5 to mice via a dose escalation protocol. Healthy nude mice were exposed daily for 1 week to incrementally increase doses of ADDA 5 up to 80 mg/kg, and weight loss and animal behavior were monitored. Acute treatment with ADDA 5 did not induce detectable toxicity in mice. The mice

were followed up for 6 months, and no toxic effects were observed.

UTMZ cells were transplanted into mice at 6 weeks of age, and after 12 days the mice were treated intraperitoneally with ADDA 5 (8 mg/kg) or DMSO-saline as a control. Tumor volume was measured once each week, starting at day 28 when tumors became visible. At 43 days, animals reached the end point and were killed, and the final tumor volume of both groups was determined (Fig. 6*D*). The tumor size and tumor volume of ADDA 5-treated tumors were significantly smaller than those of the control-treated tumors ($p < 0.0001$ and $p = 0.0002$, respectively). These data indicate that inhibition of CcO with ADDA 5 halts the growth of chemoresistant glioma tumors *in vivo*.

Structure-Activity Analysis of ADDA 5 and Analogs—To further understand the structure-activity relationship of ADDA 5, twelve structural analogs were tested for the ability to inhibit CcO activity (Table 1). Analogs in the active series contain a dihydroisoquinoline core substituted at the primary alcohol with various lipophilic groups. The most active compounds (compounds 9, 12, and ADDA 5) consist of cyclized lipophilic groups such as adamantyl (compound 12 and ADDA 5) and bicycloheptane (compound 9). Compound 10, which contains a methyl and isopropyl group in the 2 and 5 position, respectively, of the cyclohexyl ring is active, but compound 11, which has the same substitutions but in the 3 and 5 position, respectively, is inactive. Compound **6**, containing a 2-methyl cyclopropyl group, was weakly active, whereas compounds **5** and **7** were inactive; compound **8** was also only weakly active, further establishing the importance of lipophilicity to activity.

To further explore the selectivity of these inhibitors, we tested the effect of the analogs on CcO activity and cell toxicity in our chemoresistant cellular model. Under the experimental conditions tested, ADDA 5 and compound 9 specifically inhibited both CcO activity (Fig. 7*A*) and the growth of UTMZ cells (Fig. 7*B*), whereas compound 1 was inactive, suggesting that the growth inhibitory effect is dependent on inhibition of CcO activity.

We next investigated the effect of selected compounds on mitochondrial extracts from glioma stem cells (GSCs) derived from Jx22 human tissue. ADDA 5 and compound 9 each inhibited the activity of CcO from Jx22-derived GSCs, whereas compound **1** did not (Fig. 8*A*). Furthermore, histochemical analysis of Jx22-derived GSCs treated with ADDA 5 or compound 9 revealed a significant reduction in staining for CcO activity compared with that in vehicle-treated GSCs (Fig. 8*B*), indicating inhibition of CcO and reduced mitochondrial respiration after treatment. No differences were detected between compound **1** and vehicle-treated GSCs, confirming that compound **1** is inactive against CcO (Fig. 8, *A* and *B*). To quantify the histochemical data, we analyzed the absorbance of images of treated and untreated GSCs. After subtracting the background, the average absorbance (± S.D.) of images of untreated cells was 2.5 (± 0.14), 3.5 (± 0.2), and 1.1 (± 0.06) times greater than that of images of ADDA 5-, compound 9-, and compound **1**-treated cells, respectively. These results confirm that mitochondrial respiration was reduced after ADDA 5 and compound **9** treatments.

TABLE 1
Structure-activity relationship for analogs of ADDA 5

Compound #	Structure	CcO IC_{50} (μM)
1	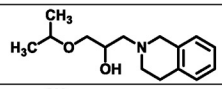	inactive
2	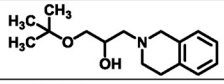	inactive
3	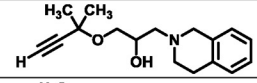	inactive
4	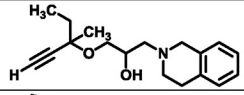	inactive
5	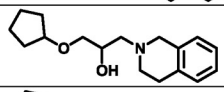	inactive
6	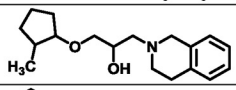	71.5
7	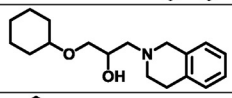	inactive
8	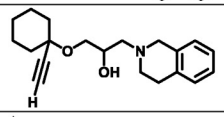	92.5
9	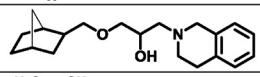	18.7
10	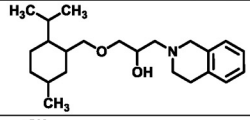	43.3
11	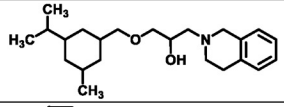	inactive
12	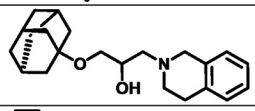	20.3
ADDA 5	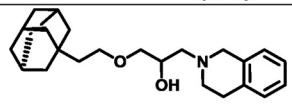	21.42

In neurosphere assays, in which Jx22 cells were dissociated and plated as single cells in Neurobasal medium, neurospheres formed in the wells treated with control (DMSO), whereas very few spheres formed from cells treated with either ADDA 5 or compound 9 (Fig. 9*A*). Moreover, in the limiting dilution assay, an *in vitro* assay that measures clonogenicity, cells grown with compound 9 or ADDA 5 had decreased self-renewal potential and formed fewer neurospheres, indicating a loss of GSC characteristic features (Fig. 9*B*). Consistent with the *in vitro* biochemical results (Fig. 8, *A* and *B*), compound **1** had no effect on self-renewal or neurosphere formation (Fig. 9, *A* and *B*).

Discussion

We recently showed that TMZ-dependent acquired chemoresistance in glioma cells may be due to a mitochondrial

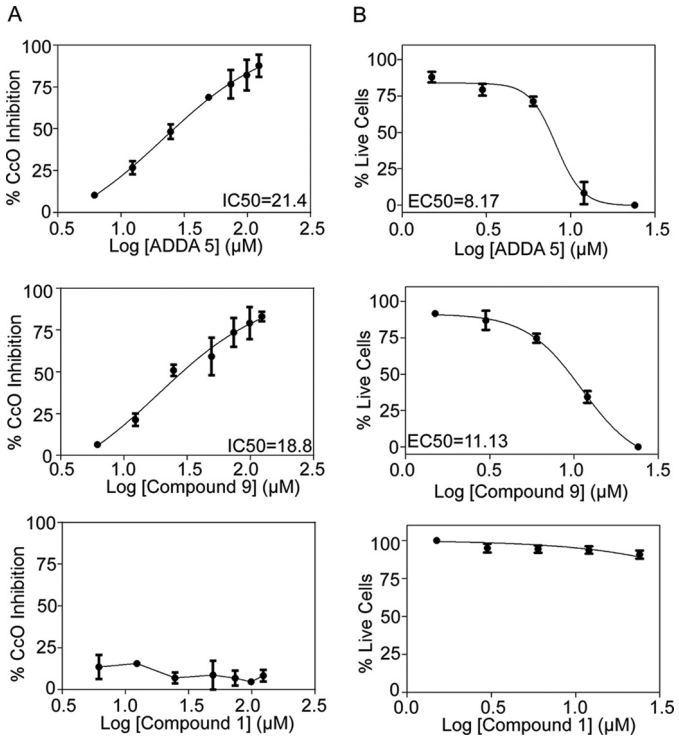

FIGURE 7. **Effect of ADDA 5 and analogs on CcO activity and proliferation of TMZ-resistant cells.** *A*, effect of ADDA 5 (*top panel*), compound 9 (*middle panel*), and compound 1 (*bottom panel*) on CcO activity in UTMZ cells. ADDA 5 and compound 9 inhibited CcO with an IC_{50} of 21.4 ± 3.9 and 18.8 ± 4.5 μM, respectively. Compound 1 was inactive against CcO. *B*, effect of ADDA 5 (*top panel*), compound 9 (*middle panel*), and compound 1 (*bottom panel*) on cell proliferation. Cells were treated with compounds at the indicated concentrations.

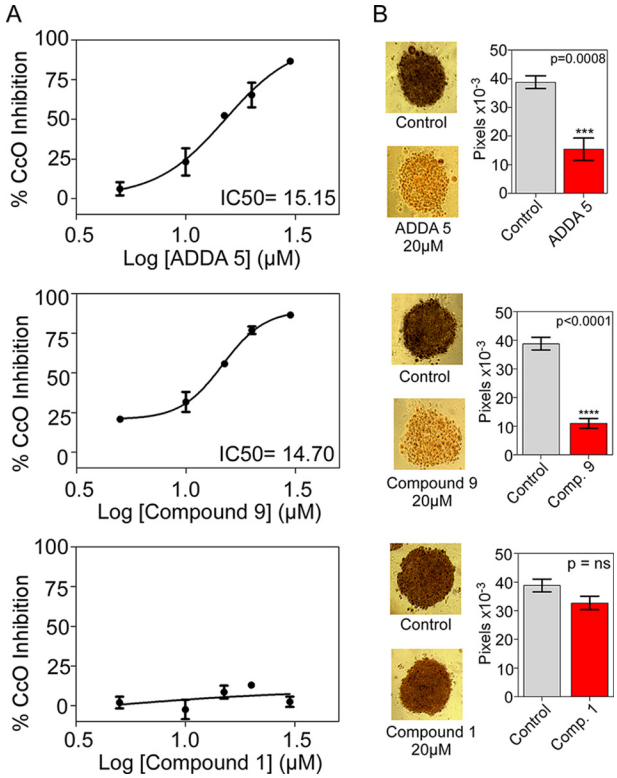

FIGURE 8. **Effect of ADDA 5 and analogs on CcO activity and proliferation of GSCs.** *A*, effect of ADDA 5 (*top panel*), compound 9 (*middle panel*), and compound 1 (*bottom panel*) on CcO activity in Jx22-derived GSCs. ADDA 5 and compound 9 inhibited CcO with an IC_{50} of 15.5 ± 2.8 and 14.7 ± 1.5 μM, respectively. Compound 1 was inactive against CcO. Cells were treated with compounds at the indicated concentrations. *B*, analysis of CcO function in control GSCs and those exposed to ADDA 5, compound 9, or compound 1. *Left panel*, representative images of GSCs grown on coverslips, air-dried, and stained for CcO activity. *Right panel*, *bar graphs* representing the average absorbance (±S.D.) of images of untreated GSCs or treated cells. Greater absorbance indicates greater CcO activity. *Comp.*, compound.

adaptive response, with a major contribution from CcO. We also showed that pharmacologic or genetic inhibition of CcO restores sensitivity to TMZ-dependent apoptosis in chemoresistant glioma cells. Most strikingly, these changes are likely to be clinically relevant because they were recapitulated in patient biopsies after adjuvant therapy with TMZ (9–11, 14). Thus, abrogation of this adaptive response may reverse chemoresistance and restore sensitivity to TMZ, providing a strategy for improved therapeutic outcomes in patients with GBM. However, there are no known CcO inhibitors that can be applied for therapeutic uses. Cyanide, sulfide, azide, and carbon monoxide all bind to the iron core within CcO, preventing transport of electrons from cyt *c* to oxygen in all mitochondria-containing cells (21, 22). As a result, the ETC is disrupted, and the cells can no longer aerobically produce ATP for energy. Tissues that depend highly on aerobic respiration, such as the central nervous system and the heart, are particularly affected (23–25); thus these compounds have a high toxicity profile. Molecules that inhibit CcO activity specifically in tumor cells may be of therapeutic benefit however.

Here, we report the discovery of a novel, small molecule noncompetitive inhibitor that shows selectivity for CcO over other respiratory chain complexes. The 135,000-compound library that was screened by HTS produced four compounds with IC_{50} values of <50 μM. A thorough redox counter screen effectively eliminated false positives and led us to discover one leading hit.

Our data show that at the tested concentrations, ADDA 5 inhibits the growth of both TMZ-sensitive and resistant glioma cell lines but does not affect growth of a non-tumorigenic cell line. Therefore, it should be possible to identify a dosage of ADDA 5 that primarily targets glioma cells, which will be critical for clinical application. In addition, the lipophilic nature of ADDA 5 might facilitate passage through the blood-brain barrier to further increase tumor targeting.

Analysis of the mechanism of inhibition showed that ADDA 5 is a non-competitive inhibitor of CcO with respect to the cyt *c* substrate, with an IC_{50} value of <15 μM against human glioma CcO. The non-competitive inhibition provides strong evidence that this small molecule inhibitor binds to an allosteric site rather than to the active site of cyt *c*.

Interestingly, kinetic studies indicate that ADDA 5 binds to and inhibits CcO but has only partial efficacy at the enzyme relative to a full inhibitor. This characteristic of ADDA 5 suggests very interesting therapeutic windows given the metabolic aberrations specifically associated with mitochondrial bioenergetic function in cancer cells, including differences in mitochondrial CcO activity. Normal mammalian cells have a relatively large excess (3–10-fold) of CcO activity (26–31); thus, in normal brain cells the CcO activity could be decreased by ~70% before major changes in mitochondrial respiration and ATP

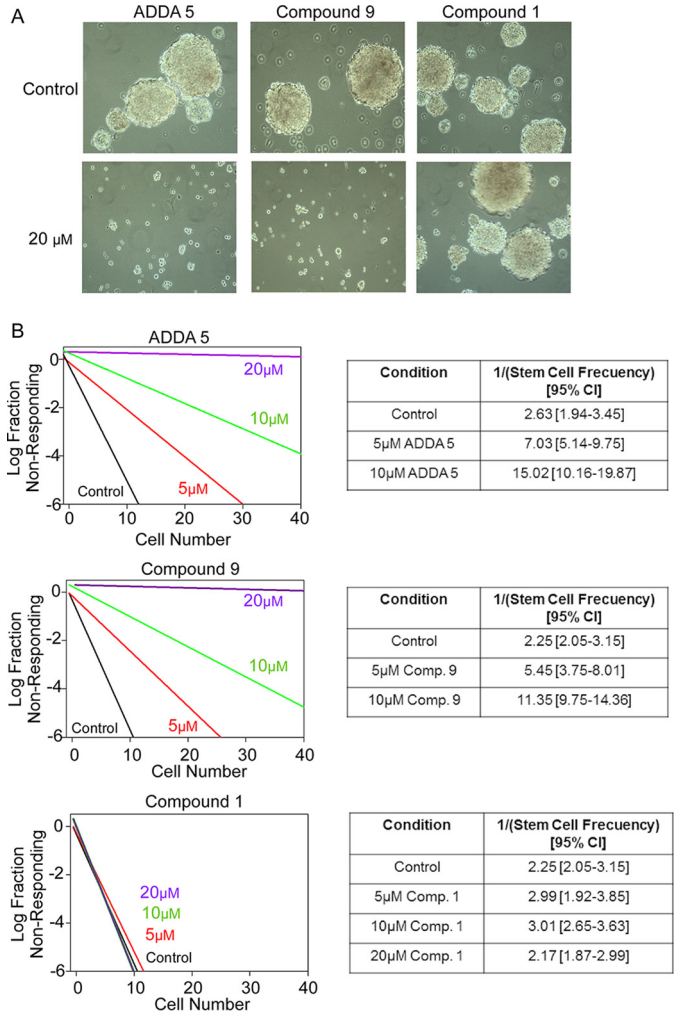

Condition	1/(Stem Cell Frecuency) [95% CI]
Control	2.63 [1.94-3.45]
5μM ADDA 5	7.03 [5.14-9.75]
10μM ADDA 5	15.02 [10.16-19.87]

Condition	1/(Stem Cell Frecuency) [95% CI]
Control	2.25 [2.05-3.15]
5μM Comp. 9	5.45 [3.75-8.01]
10μM Comp. 9	11.35 [9.75-14.36]

Condition	1/(Stem Cell Frecuency) [95% CI]
Control	2.25 [2.05-3.15]
5μM Comp. 1	2.99 [1.92-3.85]
10μM Comp. 1	3.01 [2.65-3.63]
20μM Comp. 1	2.17 [1.87-2.99]

FIGURE 9. **Effects of ADDA 5 and analogs on GSCs.** *A,* representative phase contrast photomicrographs (10× magnification) of anchorage-independent growth of Jx22-derived GSCs after 10 days of culture in serum-free Neurobasal medium supplemented with EGF and FGF and treated with ADDA 5, compound 9, or compound 1. DMSO was applied as the control. *B, in vitro* limiting dilution assays and quantification of GSCs treated with ADDA 5 (*top*), compound 9 (middle), or compound 1 (*bottom*). DMSO was applied as the control. Results represent the average from two independent experiments. Comp., compound.

synthesis occur (26, 27). Indeed, there is a very clear threshold in respiration that remains nearly maximal until a low level of CcO activity is reached. In contrast, studies have clearly shown that the CcO capacity in a variety of human cancer cell types is in low excess with respect to that required to support the endogenous respiration rate, such that a 7–22% decrease in CcO activity is sufficient to promote the alteration of energy homeostasis in malignant cells (11, 32). Therefore, the higher CcO activity and threshold in respiration in normal cells offers a therapeutic window for the use of CcO-specific inhibitors, as the effective therapeutic doses necessary to decrease CcO activity in malignant cells should not affect the maintenance of energy homeostasis in normal cells, in particular neurons and glial cells.

Our evaluation of the effects of ADDA 5 on bioenergetic function in intact glioma cells show that ADDA 5 depletes the bioenergetic reserve capacity in a concentration-dependent manner. This depletion of reserve capacity was found to be directly related to a simultaneous increase in proton-leak respiration (state 4) and decrease in ATP-linked respiration (state 3). Reserve capacity is a measure of the ability of the mitochondria to respond to physiologic stress (33, 34). Many cells operate at a basal level that only requires a part of their total bioenergetic capability. The difference between ATP produced by oxidative phosphorylation at basal activity and that at maximal activity is termed reserve respiratory capacity. Under certain conditions a tissue can require a sudden burst of additional cellular energy in response to stress or increased workload. If the reserve respiratory capacity of the cells is not sufficient to provide the required ATP, the cells risk being driven into cell death (34). Thus, through depletion of the bioenergetic reserve capacity of tumor cells, administration of these CcO inhibitors may restore chemosensitivity in tumors that have become chemoresistant (35).

Our results show that ADDA 5 and a specific analog of ADDA 5 are effective in inhibiting the growth not only of glioma cell lines, which are representative of the cells within the tumor mass, but also of GSCs, which are tumor-initiating cells capable of tumor recurrence. These data suggest that ADDA 5 and analogs would be effective in targeting the bulk of the tumor as well as in minimizing recurrence that may result from the proliferation and differentiation of cancer stem cells. Importantly, the analog that did not inhibit CcO activity did not demonstrate any effect on glioma cell line or GSC proliferation, suggesting that the cytotoxic effect of ADDA 5 and active analogs is dependent of the inhibition of CcO activity. Notably, ADDA 5 treatment substantially reduced the volume of tumors formed by chemoresistant glioma cells in mice, without any noticeable adverse effects, as indicated by a lack of change in animal weight and behavior, implying a potential therapeutic application for ADDA 5 and analogs.

In summary, we have identified a small molecule compound with significant *in vitro* and *in vivo* anti-GBM activity. The initial compound and analogs are now being optimized and pursued as drug development candidates, and if successful, the final derivative may ultimately be the first CcO-specific inhibitor for the treatment of GBM. Future optimization efforts will be focused on ADDA 5 and compound 9 in an effort to improve potency to <1 μM through further optimization of the lipophilic groups as well as modifications to the dihydroisoquinoline core. Moreover, in a broader context our study presents a new pharmacologic paradigm and may pave the way for the development of CcO-targeted therapeutics in general.

Experimental Procedures

Cell Culture—Parental U251 glioma cells and TMZ-resistant U251 cells (UTMZ) were grown in DMEM F-12 medium plus L-glutamine supplemented with 7% heat-inactivated FBS. Penicillin and streptomycin were added to the media for the HTS screening assay. Cells were incubated at 37 °C in a humidified atmosphere containing 5% CO_2. The resistant cell line was obtained by progressive adaptation of the parental TMZ-sensitive U251 cells to increasing concentrations of TMZ, as we previously described (11). LL-47 (MaDo) cells (human lung fibroblasts) were obtained from ATCC (CCL-135) and were grown according to ATCC instructions (Ham's F-12 supplemented

with 15% FBS). Culture media was supplemented with penicillin and streptomycin for the screening assay. Cell lines are grown continuously up to 10 passages, and then we started a new culture from frozen seed stocks. Cell lines are regularly tested for mycoplasma contamination using the Universal Mycoplasma Detection kit (ATCC® 30-1012K™) and authenticated by the ATCC authentication service utilizing short tandem repeat (STR) profiling.

Preparation of Mitochondria—Mitochondria were prepared as we previously described (9–11). Briefly, cells were washed twice in PBS. The pellet was resuspended in buffer (10 mm NaCl, 1.5 mm $MgCl_2$, and 10 mm Tris-HCl, pH 7.5) and then disrupted with a Dounce glass homogenizer. The homogenate was then centrifuged at 1000 × *g* for 10 min to remove cell debris, and the resulting supernatant was further centrifuged at 20,000 × *g* for 20 min. The mitochondrial pellets were washed 3 times with buffer, deep-frozen in liquid nitrogen, and stored at −80 °C until use. Mitochondria were subsequently solubilized in 10 mM potassium phosphate buffer supplemented with 0.2% *n*-dodecyl β-D-maltoside (LM) and protease inhibitors, extracted on ice for 1 h, and centrifuged at 10,000 × *g* for 10 min. The protein concentration in the supernatant was determined by the bicinchoninic acid (BCA) test. CcO content in mitochondrial extracts was determined by a spectroscopic method as previously described (6, 19, 20, 36). Briefly, mitochondrial pellets were dissolved into a 2% Triton X-100 solution to eliminate light scattering effects. The differential absorbance at 605 and 630 nm during chemically induced maximum oxidation and reduction of the sample was used to determine the absolute concentration of CcO. The oxidation of mitochondrial extracts was performed with ferricyanide, whereas the reduction was accomplished with ascorbate in combination with sodium hydrosulfite. The CcO content of mitochondria from UTMZ cells was determined to be 0.63 nmol/mg protein and 24.37 nmol/g wet mitochondrial weights.

Purification of CcO—Mitochondrial fractions from U251 human glioma cells were solubilized with 10 mM potassium phosphate buffer, pH 7.4, containing 1% LM and protease inhibitors (Buffer A). Samples were incubated on ice for 1 h with vortexing every 10 min. Samples were then centrifuged at 16,000 × *g* for 10 min, and the supernatant recovered for immunoprecipitation. Mitochondrial supernatants were precipitated using monoclonal complex IV antibody irreversibly cross-linked to protein G-agarose beads (Abcam #ab109801). Samples were immunoprecipitated overnight at 4 °C with gentle rotation. After the mixing step was complete, the beads were collected by centrifugation for 1 min at 1000 × *g*, and the beads were washed 3 times with buffer A during 10 min with rotation. To measure CcO activity, the beads were suspended in 10 mM potassium phosphate buffer, pH 7.2, containing 0.2% LM and used as the source of CcO. For SDS-PAGE, CcO subunits were eluted from the beads in 4× Laemmli sample buffer, heated at 95 °C for 5 min, and centrifuged at 1000 × *g*. The supernatant was then loaded in a 12% SDS-PAGE gel. Purified CcO from bovine heart was purchased from Sigma (catalogue #C5499).

Mass Spectrometry—After protein electrophoresis, the stained bands were excised, and the Coomassie Blue staining was removed by an overnight wash in 50% 100 mM ammonium bicarbonate, 50% acetonitrile. To reduce the disulfide bonds, the excised gel pieces were incubated in dithiothreitol (25 mM) at 50 °C for 30 min followed by incubation with iodoacetamide (55 mM) for 30 min in the dark to alkylate-free thiol groups. Excess alkylating agent was then removed, and the gel pieces were evaporated to dryness before re-swelling in 100 mM ammonium bicarbonate buffer and overnight digestion using mass spectrometry grade trypsin (12.5 ng/ml). Tryptic peptides were extracted using a solution of 1% formic acid in water and acetonitrile (50/50) and then evaporated to dryness in a SpeedVac.

For MS evaluation, samples were resuspended in 30 μl of double-distilled H_2O with 0.1% formic acid. An aliquot (5 μl) of each digest was loaded onto a Nano cHiPLC 200-μm × 0.5-mm ChromXP C18-CL 3-μm 120 Å reverse-phase trap cartridge (Eksigent, Dublin, CA) at 2 μl/min using an Eksigent 415 LC system autosampler. The cartridge was washed for 10 min with 0.1% formic acid in ddH_20, and the bound peptides then were flushed onto a Nano cHiPLC column, ChromXP C18-CL 3 μm 120 Å (Eksigent) with a 15-min linear (5–50%) acetonitrile gradient in 0.1% formic acid at 1000 nl/min using an Eksigent Nano1D+LC. The column was washed with 90% acetonitrile, 0.1% formic acid for 5 min and then re-equilibrated with 5% acetonitrile, 0.1% formic acid for 5 min. The protein digest was analyzed using the Sciex 5600 Triple-Tof mass spectrometer (Sciex, Toronto, Canada), with the IonSpray voltage at 2300 V and the declustering potential at 80 V. Ion spray and curtain gases were set at 10 p.s.i. and 25 p.s.i., respectively, and the interface heater temperature was 120 °C. Eluted peptides were subjected to a time-of-flight survey scan from 400 to 1250 *m*/*z* to determine the top 20 most intense ions for MS/MS analysis. Product ion time-of-flight scans at 50 ms were conducted to obtain the tandem mass spectra of the selected parent ions over the range from 400 to 1500 *m*/*z*. Spectra were centroided and de-isotoped by Analyst software, version 1.6 TF (Sciex). A β-galactosidase trypsin digest was used to establish and confirm the mass accuracy of the mass spectrometer.

The tandem MS data were processed to provide protein identifications using an in-house Protein Pilot 4.5 search engine (Sciex) using the *Homo sapiens*, *Bos taurus*, and *Mus musculus* UniProt protein database and using a trypsin digestion parameter. Proteins of significance were accepted on the criteria of having at least two peptides detected with a confidence score of ≥95%.

HTS Assay—A biochemical absorbance-based HTS assay measuring CcO activity in a 1536-well microtiter plate format was used to identify CcO inhibitors. The screening collection of 134,855 compounds was composed of ~100,000 chemically diverse commercially available compounds from Chembridge, ~30,000 compounds from the Enamine Diverse Collection, ~2,700 compounds of known biological activity, including approved drugs, and the Southern Research proprietary collection. The Southern Research collection and known biologically active collections were screened at 30 μM, and the commercial compounds were screened at 10 μg/ml. Compounds described in Table 1 were purchased from Chembridge; NMR files provided by the supplier can be found in supplemental Fig. S1. The assays were run at room temperature at a final volume of 5 μl

per well. The enzyme reaction was performed under the following assay buffer conditions: 10 mM potassium phosphate, pH 7.2, 0.2% *n*-dodecyl β-D-maltoside, and 2% DMSO. To initiate the reaction, 2.5 μl of reduced cyt *c* (100 μM in assay buffer) and 2.5 μl of mitochondrial extracts (20 μg/ml in assay buffer) were added to the well with a BioRaptr FRD (Beckman Coulter). The decrease in absorbance at 550 nM was measured for 4 min, and the enzymatic rate was determined using an EnVision Multilabel Reader (PerkinElmer Life Sciences). Background control wells included all reagents except mitochondrial extracts. Plates were pre-drugged with test compounds using a Labcyte ECHO 555 Liquid Handler.

Cell-based Counter Screen—The same general procedure was used for all of the cell-based screening assays. Compounds were diluted to a 6× screening concentration in assay media using a Biomek FX (Beckman), and 5 μl of diluted compound was dispensed to the assay plates. Cells were added to the plate in a total volume of 25 μl containing 1500 cells. Plates were incubated for 72 h at 37 °C, 5% CO_2, and 95% humidity. Cell viability was determined using Cell Titer Glo (Promega). The cytotoxicity assay was performed using the LL-47 cell line, the parental non-TMZ resistant (U251) cell line, and the TMZ-resistant (UTMZ) cell line, which was screened both with and without TMZ added to the assay.

Mitochondrial Complex Activities and High Resolution Respirometry—Mitochondrial complex activities were spectrophotometrically determined as previously described (9–12, 14) using mitochondrial extracts from UTMZ-glioma cells. All activities were normalized to protein content. High resolution respirometry was performed by measuring oxygen consumption in a two-channel respirometer (Oxygraph-2k with DatLab software; Oroboros Instruments, Innsbruck, Austria) as we previously described (9, 10). Statistical analysis was performed with the Student's *t* test, and $p < 0.05$ was considered statistically significant.

Kinetic Experiments—The kinetic parameters for CcO activity were determined in mitochondrial extracts using a two-channel respirometer (Oxygraph-2k with DatLab software). CcO activity was analyzed in the presence of 2 mM ascorbate, at different concentrations of cyt *c* (0.25–3 μM). Ascorbate was added as a regenerating system for reduced cyt *c*. The extent of reaction progression was followed over time, and oxygen consumption was plotted as a function of cyt *c* or inhibitor concentration. The initial portions of the reaction curves were fitted to a linear equation to approximate the pre-steady-state reaction velocities using Prism (Graphpad software). Lineweaver-Burk and Dixon plots were then generated with the pre-steady-state reaction velocities and the corresponding substrate concentrations.

Enzymatic Activities—XO activity was measured as we previously described (4) using XO from bovine milk (Sigma, catalogue #X1875); SOD activity and GPx activity were measured as previously described (3) using SOD from human erythrocytes (Sigma, catalogue # S9636) and GPx from bovine erythrocytes (Sigma, catalogue #G6137); LDH activity was measured as we previously described (37) using LDH from rabbit muscle (Sigma, catalogue #427217); GR activity was measured as previously described (27) using GR from baker's yeast (*Saccharomyces cerevisiae*) (Sigma, catalogue #G3664). Catalase activity was quantified by measuring oxygen production in a two-channel respirometer (Oxygraph-2k with DatLab software). The chambers were filled with 2 ml of 50 mM potassium phosphate buffer, pH 7.0, containing 0.036% (w/w) hydrogen peroxide. The oxygen content in the chambers was depleted to 5 nM by flushing the chambers with nitrogen. Once the baseline was stable for 5–10 min, the reaction was started by the addition of catalase (0.001 mg) and DMSO in the control chamber and the addition of catalase (0.001 mg) and ADDA 5 (at the concentration indicated in the figure) in the test chamber. Oxygen production was followed for 5 min, and the enzyme activity was calculated based on the slope of the curve.

In Vivo Studies—The *in vivo* studies were performed as we previously described (9). Briefly, 0.5×10^6 UTMZ cells were injected into the rear flank of 6-week-old nude mice (Envigo, IN). Twelve days later, 5 injections of vehicle (DMSO)/PBS or ADDA 5 (8 mg/kg in DMSO/PBS) were administered intraperitoneally every 2 days. Flank growth was monitored once each week with calipers to estimate tumor volume.

Cell Viability and Anchorage-independent Clonogenic Assays—To determine cell viability, 1×10^4 UTMZ cells per well were seeded into 96-well plate overnight. Cells were treated with various concentrations of compounds for 72 h before the addition of Alamar Blue dye and the absorbance reading at 570 nm and 600 nm. As a negative control, cells were treated with vehicle (DMSO) only. Eight replicates were performed per compound concentration, and the experiments were repeated at least three times. The EC_{50} was defined as the concentration of compound needed to reduce 50% of absorbance relative to DMSO-treated control. Anchorage-independent clonogenic assays with Jx22-derived GSCs were performed as we previously described (9, 38).

Histochemistry—Histochemical staining for CcO activity was performed as previously described (39–41). Briefly, neurospheres were seeded on a chamber slide system, and after attachment the spheres were air-dried for 1 h at room temperature. Neurospheres were then rinsed with PBS and incubated for 6 h at 37 °C with PBS containing 1 mg/ml cyt *c*, 1 mg/ml diaminobenzidine, 0.2 mg/ml catalase, and 0.25% (v/v) DMSO. The compounds were added directly to the incubation media, and DMSO was used in control wells. The coverslips were examined with a Nikon microscope with bright-field optics. Histochemical staining was quantified using Image J (National Institutes of Health) software. Ten color images were captured with ×40 objectives. All the samples were evaluated using the same threshold settings.

In Vitro Limiting Dilution Assay—In vitro limiting dilution assays were performed as we previously described (9, 23). Briefly, Jx22-derived GSCs were plated at 1, 2, 5, 10, 20, and 40 cells per well in 96-well plates. Ten days after plating, the number of neurospheres in each well and the percentage of positive wells were quantified by manual counting. Extreme limiting dilution assay analyses were performed on the data as previously described (9, 19).

Statistics—ROC analysis was performed using the ROC analysis: web-based calculator for ROC curves from Johns Hopkins University (ROC Analysis). Data were evaluated

using GraphPad. All reported p values are for two-sided t tests, and $p < 0.05$ was considered to indicate statistical significance. Experiments were performed in triplicate and performed twice or more to verify the results. Data are shown as the mean ± S.D., with $p < 0.05$ (*), $p < 0.01$ (**), and $p < 0.001$(***).

Author Contributions—C. R. O., E. L. W., M. E., M. J. S., S. M. B., and C. E. G. conceived and designed the experiments. C. R. O., T. M., L. J. R., L. R., D. R. M., and C. E. G. performed the experiments. C. R. O., W. Z., and C. E. G. analyzed the data. M. J. S. and C. E. G. contributed reagents, materials, and analysis tools. C. R. O. and C. E. G. wrote the paper.

Acknowledgments—We thank the staff of the Southern Research Institute High-Throughput Screening Center for support, especially Kanyupria Whig for execution of the cell-based HTS assays, Sara McKellip for compound management, and Melinda Sosa for data analysis and informatics support. We thank Praveen Vayalil and Kelley Smith-Johnston for execution of part of the inhibitor specificity assays. We thank Dr. Erin Thacker for professional editing of the manuscript.

References

1. Bryant, N. L., Gillespie, G. Y., Lopez, R. D., Markert, J. M., Cloud, G. A., Langford, C. P., Arnouk, H., Su, Y., Haines, H. L., Suarez-Cuervo, C., and Lamb, L. S., Jr. (2011) Preclinical evaluation of *ex vivo* expanded/activated γδ T cells for immunotherapy of glioblastoma multiforme. *J. Neurooncol.* **101,** 179–188
2. Sancho, P., Barneda, D., and Heeschen, C. (2016) Hallmarks of cancer stem cell metabolism. *Br. J. Cancer* **114,** 1305–1312
3. Weydert, C. J., and Cullen, J. J. (2010) Measurement of superoxide dismutase, catalase, and glutathione peroxidase in cultured cells and tissue. *Nat. Protoc.* **5,** 51–66
4. Griguer, C. E., Oliva, C. R., Kelley, E. E., Giles, G. I., Lancaster, J. R., Jr, and Gillespie, G. Y. (2006) Xanthine oxidase-dependent regulation of hypoxia-inducible factor in cancer cells. *Cancer Res.* **66,** 2257–2263
5. Sun, W. G., Weydert, C. J., Zhang, Y., Yu, L., Liu, J., Spitz, D. R., Cullen, J. J., and Oberley, L. W. (2010) Superoxide enhances the antitumor combination of AdMnSOD plus BCNU in breast cancer. *Cancers* **2,** 68–87
6. Schwerzmann, K., Hoppeler, H., Kayar, S. R., and Weibel, E. R. (1989) Oxidative capacity of muscle and mitochondria: correlation of physiological, biochemical, and morphometric characteristics. *Proc. Natl. Acad. Sci. U.S.A.* **86,** 1583–1587
7. Stupp, R., Mason, W. P., van den Bent, M. J., Weller, M., Fisher, B., Taphoorn, M. J., Belanger, K., Brandes, A. A., Marosi, C., Bogdahn, U., Curschmann, J., Janzer, R. C., Ludwin, S. K., Gorlia, T., Allgeier, A., *et al.* (2005) Radiotherapy plus concomitant and adjuvant temozolomide for glioblastoma. *N. Engl. J. Med.* **352,** 987–996
8. Stupp, R., van den Bent, M. J., and Hegi, M. E. (2005) Optimal role of temozolomide in the treatment of malignant gliomas. *Curr. Neurol. Neurosci. Rep.* **5,** 198–206
9. Oliva, C. R., Markert, T., Gillespie, G. Y., and Griguer, C. E. (2015) Nuclear-encoded cytochrome c oxidase subunit 4 regulates BMI1 expression and determines proliferative capacity of high-grade gliomas. *Oncotarget* **6,** 4330–4344
10. Oliva, C. R., Moellering, D. R., Gillespie, G. Y., and Griguer, C. E. (2011) Acquisition of chemoresistance in gliomas is associated with increased mitochondrial coupling and decreased ROS production. *PLoS ONE* **6,** e24665
11. Oliva, C. R., Nozell, S. E., Diers, A., McClugage, S. G., 3rd, Sarkaria, J. N., Markert, J. M., Darley-Usmar, V. M., Bailey, S. M., Gillespie, G. Y., Landar, A., and Griguer, C. E. (2010) Acquisition of temozolomide chemoresistance in gliomas leads to remodeling of mitochondrial electron transport chain. *J. Biol. Chem.* **285,** 39759–39767
12. Barrientos, A., Fontanesi, F., and Diaz, F. (2009) Evaluation of the mitochondrial respiratory chain and oxidative phosphorylation system using polarography and spectrophotometric enzyme assays. *Curr. Protoc. Hum. Genet.* 10.1002/0471142905.hg1903s63
13. Campian, J. L., Qian, M., Gao, X., and Eaton, J. W. (2004) Oxygen tolerance and coupling of mitochondrial electron transport. *J. Biol. Chem.* **279,** 46580–46587
14. Griguer, C. E., Cantor, A. B., Fathallah-Shaykh, H. M., Gillespie, G. Y., Gordon, A. S., Markert, J. M., Radovanovic, I., Clement-Schatlo, V., Shannon, C. N., and Oliva, C. R. (2013) Prognostic relevance of cytochrome C oxidase in primary glioblastoma multiforme. *PLoS ONE* **8,** e61035
15. Darley-Usmar, V. M., Capaldi, R. A., Takamiya, S., Millett, F., Wilson, M. T., MalatestaF, and Sarti, P. (1987) *Mitochondria: A Practical Approach*, IRL Press at Oxford University Press, Oxford
16. Ragan, C. I., Wilson, M. T., Darley-Usmar, V. M., and Lowe, P. N. (1987) *Mitochondria: A Practical Approach*, IRL Press at Oxford University Press, Oxford
17. Zhang, J. H., Chung, T. D., and Oldenburg, K. R. (1999) A simple statistical parameter for use in evaluation and validation of high throughput screening assays. *J. Biomol. Screen.* **4,** 67–73
18. Eng, J. (2013) Receiver operating characteristic analysis: utility, reality, covariates, and the future. *Acad. Radiol.* **20,** 795–797
19. Williams, J. N., Jr. (1964) A method for the simultaneous quantitative estimation of cytochromes a, B, C1, and C in mitochondria. *Arch. Biochem. Biophys.* **107,** 537–543
20. Harris, S. I., Balaban, R. S., Barrett, L., and Mandel, L. J. (1981) Mitochondrial respiratory capacity and Na^+- and K^+-dependent adenosine triphosphatase-mediated ion transport in the intact renal cell. *J. Biol. Chem.* **256,** 10319–10328
21. Way, J. L., Leung, P., Cannon, E., Morgan, R., Tamulinas, C., Leong-Way, J., Baxter, L., Nagi, A., and Chui, C. (1988) The mechanism of cyanide intoxication and its antagonism. *CIBA Found. Symp.* **140,** 232–243
22. Way, J. L. (1984) Cyanide intoxication and its mechanism of antagonism. *Annu. Rev. Pharmacol. Toxicol.* **24,** 451–481
23. Chen, Q., Vazquez, E. J., Moghaddas, S., Hoppel, C. L., and Lesnefsky, E. J. (2003) Production of reactive oxygen species by mitochondria: central role of complex III. *J. Biol. Chem.* **278,** 36027–36031
24. Gunasekar, P. G., Borowitz, J. L., and Isom, G. E. (1998) Cyanide-induced generation of oxidative species: involvement of nitric oxide synthase and cyclooxygenase-2. *J. Pharmacol. Exp. Ther.* **285,** 236–241
25. Jones, M. G., Bickar, D., Wilson, M. T., Brunori, M., Colosimo, A., and Sarti, P. (1984) A re-examination of the reactions of cyanide with cytochrome c oxidase. *Biochem. J.* **220,** 57–66
26. Cribb, A. E., Leeder, J. S., and Spielberg, S. P. (1989) Use of a microplate reader in an assay of glutathione reductase using 5,5′-dithiobis(2-nitrobenzoic acid). *Anal. Biochem.* **183,** 195–196
27. Tietze, F. (1969) Enzymic method for quantitative determination of nanogram amounts of total and oxidized glutathione: applications to mammalian blood and other tissues. *Anal. Biochem.* **27,** 502–522
28. Letellier, T., Heinrich, R., Malgat, M., and Mazat, J. P. (1994) The kinetic basis of threshold effects observed in mitochondrial diseases: a systemic approach. *Biochem. J.* **302,** 171–174
29. Gnaiger, E., Lassnig, B., Kuznetsov, A., Rieger, G., and Margreiter, R. (1998) Mitochondrial oxygen affinity, respiratory flux control and excess capacity of cytochrome *c* oxidase. *J. Exp. Biol.* **201,** 1129–1139
30. Sun, A. S., and Cederbaum, A. I. (1980) Oxidoreductase activities in normal rat liver, tumor-bearing rat liver, and hepatoma HC-252. *Cancer Res.* **40,** 4677–4681
31. Sun, A. S., Sepkowitz, K., and Geller, S. A. (1981) A study of some mitochondrial and peroxisomal enzymes in human colonic adenocarcinoma. *Lab. Invest.* **44,** 13–17
32. Villani, G., Greco, M., Papa, S., and Attardi, G. (1998) Low reserve of cytochrome *c* oxidase capacity *in vivo* in the respiratory chain of a variety of human cell types. *J. Biol. Chem.* **273,** 31829–31836
33. Sansbury, B. E., Jones, S. P., Riggs, D. W., Darley-Usmar, V. M., and Hill, B. G. (2011) Bioenergetic function in cardiovascular cells: the importance

of the reserve capacity and its biological regulation. *Chem. Biol. Interact.* **191,** 288–295
34. Dranka, B. P., Hill, B. G., and Darley-Usmar, V. M. (2010) Mitochondrial reserve capacity in endothelial cells: the impact of nitric oxide and reactive oxygen species. *Free Radic. Biol. Med.* **48,** 905–914
35. Reily, C., Mitchell, T., Chacko, B. K., Benavides, G., Murphy, M. P., and Darley-Usmar, V. (2013) Mitochondrially targeted compounds and their impact on cellular bioenergetics. *Redox Biol.* **1,** 86–93
36. Balaban, R. S., Mootha, V. K., and Arai, A. (1996) Spectroscopic determination of cytochrome c oxidase content in tissues containing myoglobin or hemoglobin. *Anal. Biochem.* **237,** 274–278
37. Griguer, C. E., Oliva, C. R., and Gillespie, G. Y. (2005) Glucose metabolism heterogeneity in human and mouse malignant glioma cell lines. *J. Neurooncol.* **74,** 123–133
38. Griguer, C. E., Oliva, C. R., Gobin, E., Marcorelles, P., Benos, D. J., Lancaster, J. R., Jr., and Gillespie, G. Y. (2008) CD133 is a marker of bioenergetic stress in human glioma. *PLoS ONE* **3,** e3655
39. Partridge, M. A., Huang, S. X., Hernandez-Rosa, E., Davidson, M. M., and Hei, T. K. (2007) Arsenic induced mitochondrial DNA damage and altered mitochondrial oxidative function: implications for genotoxic mechanisms in mammalian cells. *Cancer Res.* **67,** 5239–5247
40. Salviati, L., Hernandez-Rosa, E., Walker, W. F., Sacconi, S., DiMauro, S., Schon, E. A., and Davidson, M. M. (2002) Copper supplementation restores cytochrome *c* oxidase activity in cultured cells from patients with SCO2 mutations. *Biochem. J.* **363,** 321–327
41. Melendez-Ferro, M., Rice, M. W., Roberts, R. C., and Perez-Costas, E. (2013) An accurate method for the quantification of cytochrome *c* oxidase in tissue sections. *J. Neurosci. Methods* **214,** 156–162